IVYSPRING INTERNATIONAL PUBLISHER

*International Journal of Biological Sciences*

2027; 23(1): 1-18. doi: 10.7150/ijbs.125549

Research Paper

# An RGD-Dependent ROBO1-Integrin αvβ1 Axis Promotes Liver Fibrosis in Metabolic Dysfunction-Associated Steatohepatitis

Tian Tian[1#], Martin Nzegwu[1#], Alexander Mrozek[2#], Yuhua Xue[1], Chunbao Sun[1], Arina Zhirkova[1], Mahfuza Mannan[1], Rineetha Tandra[3], Hua Lu[2], Heewon Park[2], Liya Pi[1]✉

1. Department of Pathology, Tulane University School of Medicine, New Orleans, LA, USA.
2. Department of Biochemistry and Molecular Biology, and Tulane Cancer Center, Tulane University School of Medicine, New Orleans, LA, USA.
3. Baton Rouge General Medical Center, Baton Rouge, LA, USA.

# co-first authors with equal contribution.

✉ Corresponding author: Liya Pi, PhD, Department of Pathology, Tulane University School of Medicine, 1430 Tulane Ave, New Orleans, LA, USA; Email: lpi@tulane.edu; Phone: (504)-988-2869.

© The author(s). This is an open access article distributed under the terms of the Creative Commons Attribution License (https://creativecommons.org/licenses/by/4.0/). See https://ivyspring.com/terms for full terms and conditions.

Received: 2025.09.20; Accepted: 2026.08.20; Published: 2027.01.01

## Abstract

**Background:** Roundabout (ROBO)1 belongs to the immunoglobulin (Ig) superfamily of cell adhesion molecules and has emerging roles in liver fibrosis. This study aimed to dissect profibrotic signaling mediated by ROBO1 during metabolic dysfunction-associated steatohepatitis (MASH).

**Methods:** ROBO1 expression was examined using livers of MASH patients and animals that were fed a choline-deficient, high-fat, L-amino acid–defined high fat diet (CDAHFD). Hepatic stellate cells (HSCs)-specific *Robo1* function was analyzed using knockouts (KO) in which exon 3 was deleted via *Lrat*-Cre in floxed homozygotes. Soluble N-terminal ectodomain carrying an RGD (arginine-glycine-aspartic acid) motif (ROBO1N:Fc) or an RGA (arginine-glycine-alanine) mutant in Fc chimera (mutant:Fc) was ectopically expressed in recombinant adeno-associated virus serotype 8 (AAV8), and their antifibrotic activities were compared *in vitro* and *in vivo*.

**Results:** ROBO1 and its ligand Slit guidance ligand 2 (SLIT2) were induced in advanced MASH of clinical samples and CDAHFD-fed mouse livers, while its HSC-specific deletion attenuated the MASH-fibrosis after 12-week CDAHFD feeding. Mechanistically, ROBO1 contained an RGD motif within its Ig3 domain that mediates high-affinity binding to integrin αvβ1. Concurrent engagement of ROBO1 and αvβ1 via stimulation by their ligands SLIT2 and connective tissue growth factor (CTGF) caused phosphorylation of phosphatidylinositol 3-kinase (PI3K), protein kinase B (AKT), and β-Catenin. Mutation of the RGD motif to RGA disrupted the ROBO1/αvβ1 binding and reduced activation of the PI3K/AKT/β-Catenin signaling in HSC and CDAHFD-fed livers. Additionally, the ROBO1N:Fc chimera significantly downregulated fibrosis-related genes, reduced HSC activation, and attenuated collagen deposition, whereas the RGA mutant lost these antagonistic effects on MASH-associated fibrosis.

**Conclusions:** ROBO1 binds to integrin αvβ1 via a novel RGD motif critical for HSC activation and MASH-associated liver fibrosis. Targeting this RGD-mediated interaction represents a promising strategy for antifibrotic intervention in advanced MASH.

Keywords: SLIT2/ROBO1 pathway; CTGF/integrin αvβ1; hepatic stellate cells; liver fibrosis; MASH

## Introduction

Metabolic dysfunction-associated steatotic liver disease (MASLD) is rapidly emerging as one of the most prevalent forms of chronic liver disease, primarily driven by the rise in obesity and type 2 diabetes globally [1]. MASLD includes a range of liver disorders, from steatosis to metabolic dysfunction-

associated steatohepatitis (MASH), which was formerly known as nonalcoholic steatohepatitis (NASH), and can advance to fibrosis, cirrhosis, and ultimately hepatocellular carcinoma (HCC) [2]. Chronic nutritional overload in MASLD leads to sustained hepatocellular injury, thereby activating hepatic stellate cells (HSCs) as part of the liver's wound-healing response. Once activated, HSCs often differentiate into myofibroblast-like cells, producing excessive extracellular matrix (ECM) components, particularly collagen, ultimately contributing to liver fibrosis and scarring. Advanced stages of MASLD, including cirrhosis and HCC, frequently necessitate liver transplantation and account for a substantial portion of liver-related mortality. So far, there is an unmet clinical need for therapies that target the core fibrogenic mechanisms rather than metabolic drivers alone. Resmetirom is the Food and Drug Administration (FDA)-approved therapy for MASH, but it demonstrates only modest improvements in liver fibrosis [3]. Recently, Semaglutide was subsequently approved by FDA as the first glucagon-like peptide-1 (GLP-1) therapy for MASH patients with moderate to advanced liver fibrosis, showing superior results in resolving MASH compared to placebo [4]. Treatment with Survodutide [a dual glucagon receptor/GLP-1 receptor agonist] [5] or Tirzepatide [a dual glucose-dependent insulinotropic polypeptide receptor (GIPR)/GLP-1 agonist] shows some improvement in MASH-associated liver fibrosis [6].

Integrins are the principal cell adhesion receptors that mediate interactions between cells and the ECM [7]. These heterodimeric transmembrane proteins play a dual role by sensing both the chemical and physical cues from the ECM by binding extracellularly to matrix components and intracellularly to the cytoskeleton, thus forming a critical mechanical and biochemical linkage between the extracellular environment and the cell interior. A subset of integrins can specifically recognize the arginine-glycine-aspartic acid (RGD) tripeptide motif, a conserved sequence implicated in cell adhesion and signal transduction [7]. Several RGD-binding integrins are particularly important in fibrosis because they can activate transforming growth factor (TGF)-β1, a master regulator of tissue fibrosis. Among these, αv integrins are of special interest due to their prominent roles in fibrotic diseases [8]. αvβ1 is a promiscuous integrin expressed on myofibroblasts [9, 10]. Importantly, therapeutic inhibition of αvβ1 has shown efficacy in attenuating experimental fibrosis across multiple organ systems, and its suppression is being investigated in ongoing clinical trials for fibrotic diseases such as idiopathic pulmonary fibrosis and MASH [8, 11], underscoring the therapeutic potential of integrin-targeted anti-fibrotic strategies.

Roundabout (ROBO) receptors, comprising four isoforms (ROBO1-4), are members of the immunoglobulin (Ig) superfamily of cell adhesion molecules. Initially characterized as a chemorepellent receptor involved in axon guidance and leukocyte migration [12-14], ROBO1 receptor has since been recognized for its emerging roles in liver fibrosis and cancer progression [15]. This receptor can signal through its slit guidance ligand 2 (SLIT2) and activate the phosphatidylinositol 3-kinase (PI3K)/protein kinase B (AKT) pathway in HSCs, thereby contributing to fibrotic responses during liver injury [16-20]. ROBO1 signaling is enhanced through SLIT2 binding to connective tissue growth factor (CTGF, also termed CCN2) [17]. CTGF is a ligand for multiple subtypes of integrins (i.e., αvβ1 and αvβ3) [21, 22], and mediates adhesive signaling to promote HSC adhesion. So far, the crosstalk between SLIT2/ROBO1 and CTGF/integrin signaling in MASH remains poorly understood. In this study, we detected a significant and progressive upregulation of ROBO1 in human and mouse liver tissues during advanced MASH development. HSC-specific loss of this receptor reduced liver fibrosis in the experimental MASH induced by a choline-deficient L-amino acid-defined high-fat diet (CDAHFD). Also, we identified a conserved RGD motif within the Ig3 domain of ROBO1, which facilitated direct interaction with integrin αvβ1, thereby promoting HSC activation and liver fibrosis induced by CDAHFD in mice.

## Materials and Methods

### Human tissue and animal experimentation

Human liver samples with MASH were ordered from Sekisui XenoTech (Kansas City, KS) and subjected to immunohistochemical analysis (IHC) for ROBO1. In animal experimentation, *Robo1* floxed mice (Shanghai Animal Model Inc, Shanghai, China) were crossed with lecithin:retinol acyltransferase (*Lrat*)-*Cre* mice (Jackson lab, Bar Harbor, ME). Floxed homozygotes carrying *Lrat-Cre* were generated after more than 6 backcrosses. At 8 weeks of age, these floxed homozygotes with or without *Lrat-Cre* were fed CDAHFD (60 kcal% fat, no added choline, and 0.1% Methionine, Research diet, New Brunswick, NJ) for 12 weeks to induce MASH-associated liver fibrosis according to previous reports [23]. Blood and liver tissues were collected under deep anesthesia and subjected to biochemical, histological, and molecular analyses.

For ectopic expression of the N-terminal ectodomain of human ROBO1 (Genbank: NM_

133631.4), the cDNA sequences corresponding to amino acids 57-354 were added to 5′ end of human Fc chimera (termed ROBO1N:Fc) in pUC57 plasmid from GenScript Biotech (Piscataway, NJ). The ROBO1N:Fc fragment was then cloned into *EcoRI* and *XhoI* sites in the pAAV plasmid after the chicken β-actin (CBA) promoter. A mutant containing a single amino acid substitution (D288A), in which the RGD motif was mutated to RGA tripeptides in an Fc chimera (termed mutant:Fc), was also generated through site-directed mutagenesis using primers 5′ GGCCCGAGGTGA CCC 3′ (sense) and 5′ GGCCCGAGGTGCCCC 3′ (antisense) as well as the Q5 Site-Directed Mutagenesis Kit according to the manufacturer's instructions (New England Biolab, Burlington, Massachusetts). The mutant was verified by DNA sequencing. These pAAV plasmids were co-transfected into HEK293 cells with plasmids expressing Rep/Cap genes and phelper plasmids for viral packaging. AAV8 viruses expressing ROBO1N:Fc, AAV8-RGA mutant, or GFP control ($5x10^{11}$ genomic particles) were injected via the tail veins into 8-week-old C57BL/6 wild-type mice followed by the CDAHFD feeding. Twelve weeks later, blood and liver tissue were collected for analysis. All animal experiments in this study were approved by the Animal Care and Usage Committee of Tulane University and were conducted in compliance with the guidelines.

## RNA isolation and reverse transcriptase-polymerase chain reaction

Total RNA isolation and quantitative reverse transcriptase-polymerase chain reaction (qRT-PCR) analyses were performed under the same conditions as described in our previous publication [24]. Mouse primers included: 5′ GGCTCACCCCTGGATGATAA 3′ (forward) and 5′ AAAACGGTTAGCTCTGCGAC 3′ (reverse) for *Robo1* gene; 5′ GTCTTCACACTGGTG CAGCC 3′ (forward) and 5′ ACTGGAAGACACATT TGGCC 3′ (reverse) for *Ctgf*; 5′ TGTGTTCCCTAC TCAGCCGTCT 3′ (forward) and 5′ CATCGGTCA TGCTCTCTCCAA 3′ (reverse) for *Col1a2 (Collagen type I alpha 2 chain)*; 5′ TTACTTGTACAGCTCGTCCATG 3′ (forward) and 5′ GCCACCATGGTGAGCAAGGG 3′ (reverse) for *a smooth muscle actin* (*aSMA*); and 5′ TTGACGGAAGGGCACCACCAG 3′ (forward) and 5′ GCACCACCACCCACGGAATCG 3′ (reverse) for 18S ribosomal RNA gene. All qRT-PCR experiments were conducted in triplicate and analyzed using the delta-delta CT method and normalized against the reference gene (18S) for each sample.

## Expression and purification of His-tagged ROBO1 Ig3 and mutant, Solid Phase Binding Assay, and Surface Plasmon Resonance

The DNA fragments encoding the human wild-type ROBO1 Ig3 (residues V253-V354, termed ROBO1 WT-Ig3) and the RGA mutant (termed mutant-Ig3), each with an N-terminal 6xHis-tag, were cloned into the pET28a vector, and their sequences were verified. The His-tagged fusion proteins were expressed in *E. coli* Origami 2 (DE3) cells (Novagen, Madison, WI) growing in Luria Broth supplemented with 50 μg/mL of kanamycin. Cells grew until the $OD_{600}$ reached ~0.6. Fusion protein was induced with 0.2 mM isopropyl β-D-1-thiogalactopyranoside (Thermo Scientific, Waltham, MA) at 18 °C. Cells were harvested 18 hours post-induction and were resuspended in binding buffer containing 20 mM HEPES and 150 mM NaCl (pH 7.4) supplemented with 1 mM phenylmethyl sulfonyl fluoride, 1 mM benzamidine, and 0.1% IGEPAL CA-630 and lysed by sonication. Lysates were enriched by centrifugation at 12,000 *x* g for 20 minutes at 4 °C, and the supernatant was transferred to a 5 mL column of Ni-NTA agarose column (Thermo Scientific) pre-equilibrated with binding buffer. The column was washed stepwise with the binding buffer containing increasing imidazole concentrations (5 mM, 20 mM, 50 mM), and proteins were eluted with 250 mM imidazole in the same buffer. The eluate was further purified by size-exclusion chromatography on a HiLoad 26/600 Superdex 200 pg column (Cytiva, Marlborough, MA) equilibrated with the binding buffer. Target fractions were analyzed by SDS-PAGE, pooled, and concentrated to 20 mg/mL using 3 kDa MWCO centrifugal filters (Amicon, Miami, FL), flash frozen, and stored at -80 °C until further use. All chromatography purification steps were performed using an Äkta FPLC (Cytiva) system at 20 °C.

For solid phase binding assays, 96-well microtiter plates (Fisher Scientific) were coated with purified ROBO1-Ig3, mutant-Ig3, or bovine serum albumin (BSA) (0-5 μg/well) in Tris-buffered saline (TBS)-T buffer (50 mM Tris-HCl, 150 mM NaCl, pH 7.4) containing 0.05% Tween 20. The plates were then blocked with Tween 20 and 1% BSA before incubation with 10 μg/mL of biotinylated integrin αvβ1 or αvβ3 (Acro Biosystems, Newark, DE) for 16 hours. After washing with TBS, bound integrins were detected using streptavidin-conjugated horseradish peroxidase (HRP) and tetramethylbenzidine substrate (R&D Systems, Minneapolis, MN). Absorbance at 450 nm was measured using a TECAN microplate reader (Morrisville, NC).

Surface plasmon resonance (SPR) was performed on a Biacore T200 system (Cytiva) at 25 °C with data acquired at 1 Hz. Integrins αvβ1 and αvβ3 (Sino

Biological Inc, Houston, TX) were immobilized on CM5 sensor chips via amine coupling per the manufacturer's instructions. A reference channel was prepared similarly without integrins. Purified ROBO1 Ig3 WT and mutant proteins were thawed, diluted in SPR running buffer (10 mM HEPES, pH 7.4, 150 mM NaCl, 1 mM $MgCl_2$, 1 mM $MnCl_2$, 5 mM n-octyl-β-D-glucoside), and subjected to a six-point, twofold dilution series. Multi-cycle kinetics were recorded by injecting the analyte onto the sensor surface at 30 µL/min with a 1-minute association and 10-minute dissociation phase. Buffer-only injections served as blanks. Sensorgrams were reference- and blank-subtracted and globally fit to a 1:1 binding model using BIAevaluation 3.1 software (Cytiva). Representative sensorgrams were generated using GraphPad Prism (v10.4.0) (San Diego, CA).

## Immunoprecipitation and Western blotting analyses

For immunoprecipitation studies of ROBO1/integrin αvβ1 interactions, we used human HSC LX-2 cells that stably expressed HA-tagged integrin αvβ1. This was achieved by co-transfecting an HA-tagged human ITGB1 cDNA in the pCMV3 vector (Sino Biologicals, Paoli, PA) and the ITGAV gene from the mApple-Alpha-V-Integrin-25 plasmid (Addgene, Watertown, MA), followed by selection with hygromycin B and G418, respectively. Stable cells were maintained in DMEM supplemented with 10% fetal bovine serum (FBS), 1× penicillin-streptomycin, 50 µg/mL hygromycin B, and 200 µg/mL G418. Full-length human ROBO1 cDNA fused with a V5 epitope (ROBO1:V5) was cloned into the pLVX vector (Takara Bio, San Jose, CA). The RGA mutant (mutant:V5) was generated by site-directed mutagenesis described above. These constructs or the pLVX vector (250 ng) were transfected into the integrin-expressing LX-2 stable cells using Lipofectamine 3000 (Invitrogen, Waltham, MA). After 48 hours, cells were stimulated with Mock, 200 ng/mL recombinant human SLIT2 fused with a C-terminal Myc tag (SLIT2:Myc), or 200 ng/mL recombinant rat CTGF carrying three FLAG epitopes (CTGF:FLAG). SLIT2:Myc (in pSecTag2) and CTGF:FLAG (in pIRES2) were expressed in CHO cells as previously described [17, 25, 26]. SLIT2 was purified from conditioned media using anti-c-Myc agarose and eluted with c-Myc peptide (Thermo Fisher Scientific). CTGF was purified using M2 antibody-conjugated agarose and eluted with FLAG peptide (Sigma, St. Louis, MO) as described previously [26]. Two days after the ligand stimulation, cells were lysed in RIPA buffer with protease inhibitor cocktail (Sigma). For immunoprecipitation, lysates were incubated with anti-V5 tag agarose (Sigma) for 16 hours, washed in RIPA buffer, and eluted in 1× Laemmli buffer. About 30 µg protein lysates were electro-transferred to polyvinylidene difluoride (PVDF) membranes (Bio-Rad Laboratories, Hercules, CA). Immunoblotting was performed with the following antibodies: anti-V5, anti-HA, and anti-Myc from Proteintech (Rosemont, IL), and M2 antibody (Sigma). Signal detection was carried out using HRP-conjugated secondary antibodies (Santa Cruz Biotechnology, Dallas, TX) and the ECL Plus kit (Amersham Biosciences, Piscataway, NJ).

Immunoprecipitation assays were also performed using primary HSC isolated after liver perfusion in the two-step collagenase perfusion method, as previously described [25]. Specifically, *in situ* perfusion of mouse livers was carried out in EGTA solution (Sigma). Minced liver tissues were digested with 0.038% Collagenase D (Roche Applied Science, Indianapolis, IN), 40 pg/mL Pronase E (Roche Applied Science), and 0.1 mg/mL DNase I (Sigma). Hepatocytes were removed at 50 x g. Nonparenchymal (NPC) fraction was collected at 1200 rpm and suspended in single cells. Primary HSC was collected from the white layer after centrifugation at 1400 x g for 20 min in 8% Nycodenz (Sigma). Isolated HSC cells were cultured in DMEM containing 10% FBS and antibiotics. In parallel, the isolated cells were lysed in RIPA buffer with protease inhibitors. Lysates were incubated overnight with anti-human IgG (Fc-specific) agarose (Sigma). Immunocomplexes were washed extensively with cold RIPA buffer, resolved by 8% SDS-PAGE, and probed with a rabbit integrin Alpha V + Beta1 (αvβ1) antibody (Bioss Antibodies, Woburn, MA). Total input was analyzed based on immunoblotting with the rabbit integrin αvβ1 antibody and a goat anti-human Ig Fc antibody (Abcam).

Immunoblottings were performed to analyze total protein lysates or nuclear fractions isolated by NE-PER™ Nuclear Extraction Reagents (ThermoFisher Scientific) from the human and mouse HSCs or liver tissues. To assess cytosolic contamination, GAPDH (Proteintech) was used to probe the isolated nuclear fractions that were electro-transferred onto PVDF membranes, followed by staining with 0.1% Ponceau S (Sigma). Primary rabbit antibodies detected phosphorylation of PI3 Kinase regulatory subunit (p85) (p-PI3K) (Cell Signaling Technology, Danvers, MA), AKT (Cell Signaling Technology), phosphorylated β-Catenin at Serine 552 (p-β-Catenin) (Proteintech), β-Catenin (Proteintech), phosphorylated Smad3 at Serine 423 and 425 (p-Smad3) (Thermo Fisher Scientific), Slit2 (Proteintech), Robo1 (Proteintech), Histone H3 (Proteintech), and Vinculin (Proteintech). In addition, primary mouse

antibodies were ordered from Proteintech and examined PI3K p85 alpha subunit, phosphorylated AKT at Serine 473 (p-AKT), and β-actin. Detection was carried out using HRP-conjugated secondary antibodies and the Amersham ECL Plus kit (Cytiva).

### Histological analysis, Immunofluorescent staining, and Proximity Ligation Assay

Histological analysis of liver tissues was conducted on 6-μm paraffin-embedded sections. ROBO1 was stained on human liver sections with a mouse antibody (Thermo Fisher Scientific) and visualized with the ABC-Elite kit and ImmPACT DAB substrate (Vector Laboratories, Newark, CA). In addition, immunofluorescent staining on fixed mouse livers was performed using the mouse ROBO1 antibody and M.O.M kit (Vector Laboratories) in combination with the rabbit αSMA antibody described in Western blotting. Fluorescent signals were detected with Alexa Fluor 594 anti-rabbit and Alexa Fluor 488 anti-mouse secondary antibodies (Thermo Fisher Scientific). Furthermore, CDAHFD-fed livers were analyzed with the rabbit αSMA antibody in DAB staining. Collagen deposition was assessed via Sirius Red staining.

Proximity Ligation Assays (PLA) were performed using the DuoLink in Situ-Red Starter Kit (Sigma) according to the manufacturer's protocol. The rabbit integrin αvβ1 antibody and the mouse ROBO1 antibody described above were used as primary antibodies. Slides were incubated with PLA probes, followed by ligation and amplification reactions as previously described [27]. Nuclei were counterstained with DAPI in mounting medium. Images were captured using an Olympus BX51 upright fluorescence microscope equipped with an Olympus DP80 camera, Plan Fluorite objectives, and an LED transmitted-light source (Olympus, Waltham, MA). Data were analyzed based on ten random fields (200x magnification). Positively stained regions in each field were outlined and measured in pixels using ImageJ software. The fraction of positive staining was calculated relative to total pixels per image. For morphometric analysis, at least ten randomly selected fields per slide and four to five animals per group were analyzed using ImageJ and IHC Profiler software (http://rsb.info.nih.gov/ij/) according to published methods [28].

### Measurement of serum transaminases and hepatic hydroxyproline

Alanine aminotransferase (ALT) and aspartate aminotransferase (AST) were measured in the serum of animals using kits (Sigma) according to the manufacturer's instructions. In addition, hepatic hydroxyproline content was quantified calorimetrically in flash-frozen murine liver samples. Concentrations were measured from a standard curve using pure hydroxyproline (Sigma) and counted as micrograms of hydroxyproline for every gram of liver according to our previous report [17].

### Flow cytometry

Primary hepatocytes and HSCs were generated as described above by the two-step collagenase perfusion method [25]. Liver sinusoidal endothelial cells (LSEC) and macrophages were generated from mouse livers according to previous reports [29]. Cell viability was determined with the Zombie Aqua™ Fixable Viability Kit (BioLegend, San Diego, CA). Single cells were incubated with anti-mouse CD16/CD32 (BioLegend) for 10-15 minutes on ice to minimize non-specific antibody binding. Cell-specific antibodies from BioLegend included: an APC-conjugated mouse PDGFRβ antibody for HSC labeling; a 700-conjugated CD45, APC-CY7-conjugated CD11b, and PE-Dazzle594-conjugated F4/80 mouse antibodies for macrophage labeling. APC-conjugated anti-mouse VEGFR2 (BioLegend) was used for LSEC labeling. Robo1 was stained with the mouse antibody described above, followed by FITC-conjugated anti-mouse secondary antibody (Invitrogen). Flow cytometry data were collected on a LSRFortessa cytometer (BD Biosciences, San Jose, CA) using FACSDiva v.9 software (BD Biosciences) and analyzed using FlowJo v.10 (Tree Star Inc, Ashland, OR).

### Statistical analysis

GraphPad Prism 9.0 was used for statistical analysis. Statistical significance ($*P < 0.05$, $**P < 0.01$, $***P < 0.001$, $****P < 0.0001$) was evaluated using the unpaired Student *t*-test.

## Results

### ROBO1 is induced in activated HSCs and correlates positively with liver fibrosis progression in MASH

Liver fibrosis represents a common pathological endpoint for most chronic liver diseases, including MASLD. While early-stage fibrosis may still be reversible, the transition to advanced stages, particularly cirrhosis, is typically irreversible, ultimately resulting in organ failure and increased mortality. Therefore, a critical clinical priority is to identify molecular pathways and cellular targets that drive the fibrogenic process during the early and intermediate phases, when therapeutic intervention may still halt or reverse disease progression.

Comparison of liver gene expression profiles between patients with mild (n = 40, fibrosis stage 0-1) and advanced fibrosis (n = 32, fibrosis stage 3-4) revealed significant upregulation of *ROBO1* (Genbank accession#BF059159, 1.49-fold), *SLIT2* (Genbank accession#AI963304, 1.08-fold), *CTGF* (Genbank accession#M92934, 1.35-fold), and *COL1A2* gene (Genbank accession#AA628535, 1.19-fold) (Fig. 1A). In contrast, no difference was found in *ROBO2* (Genbank accession#BE858548), *ROBO3* (Genbank accession #NM_022370), *ROBO4* (Genbank accession #AA156022), *SLIT1* (Genbank accession#NM_003061), and *SLIT3* genes (Genbank accession#AB011538) (Supplementary Figure S1). Notably, *ROBO1* expression positively correlated with *COL1A2* levels (Fig. 1B), consistent with a potential profibrotic role in MASH. IHC confirmed elevated expression of ROBO1 protein in liver tissues from MASH patients compared with normal controls (Fig. 1C). In the CDAHFD dietary model that induces rapid progressive fibrosis in experimental MASH[23], we observed temporal upregulation of *Robo1*, *Ctgf*, *aSMA*, and *Col1a2* from week 1 through week 9 during CDAHFD feeding compared to chow diet-fed and age-matched controls in rats (Fig. 1D). Consistently, immunoblot analysis showed increased levels of Robo1, Ctgf, αSMA, and type I collagen proteins in 12-week CDAHFD-fed mice (Fig. 1E). Sirius Red staining confirmed elevated deposition of collagen in the CDAHFD-fed livers (Fig. 1F). Flow cytometrical analysis suggested that this 12-week CDAHFD feeding was associated with upregulation of Robo1 protein in primary hepatocytes and PDGFRβ$^+$ HSC, but not in CD11b$^+$ F4/80$^+$ macrophages and VEGFR2$^+$ LSEC (Fig. 1G). Further immunofluorescent staining labeled Robo1 protein on the majority of αSMA$^+$ HSCs and small subsets of hepatocytes in the CDAHFD-fed livers (Fig. 1H and 1I, Supplementary Figure S2 and S3), positioning HSC as the primary site of Robo1-mediated signaling during hepatic fibrogenesis in MASH.

## HSC-specific deletion of Robo1 attenuates MASH-associated liver fibrosis

Building on the observation that Robo1 is upregulated in activated HSCs during MASH progression (Fig.1G and Supplementary Figure S2), we hypothesized that genetic ablation of this receptor in HSCs would mitigate liver fibrosis. To test this hypothesis, we generated HSC-specific *Robo1* KO carrying floxed homozygotes and *Lrat-Cre*. Despite residual mRNA of *Robo1* in non-HSC cell types (i.e., hepatocytes), qRT-PCR analysis showed that KO mice displayed 34.2% reductions of *Ctgf*, 34.4% decreases of *aSMA* and 23.4% downregulation of *Col1a2* mRNA upon 12-week CDAHFD feeding (Fig. 2A). Immunofluorescent staining for Robo1 and αSMA confirmed decreased HSC activation in *Robo1* KO livers (Fig. 2B). Immunoblotting further validated reduced levels of Ctgf, αSMA, and collagen proteins in the *Robo1* KO mice compared to controls (Fig. 2C). Additional Sirius Red staining revealed reduced collagen deposition and quantitative measurement verified a 36.4% decrease in hydroxyproline content of the CDAHFD fed *Robo1* KO livers (Fig. 2D and E). Ballooning hepatocytes were detected by H&E staining in both CK and KO mice after CDAHFD treatment (Fig. 2F), while reduced ratios of the liver-to-body weight were found in KO mice compared to CK controls (Fig. 2G). Moreover, CDAHFD treatment led to higher serum ALT and AST levels in CK mice than in KO animals (Fig. 2H). These results indicate that Robo1 promotes HSC activation during MASH, as its deletion in HSCs significantly attenuates liver fibrosis.

## ROBO1 contains an RGD motif for binding to integrin αvβ1 that is highly upregulated in advanced fibrosis of human MASH

To elucidate the molecular mechanism(s) for ROBO1's pro-fibrotic function, we first analyzed its protein sequence and domain architecture. ROBO1 comprises five Ig domains (Ig1-Ig5) and three fibronectin (Fn) type III repeats. Interestingly, we identified an RGD motif within the Ig3 domain of ROBO1 in both humans and mice, a canonical binding sequence for integrins (Fig. 3A). Notably, this motif is absent in the ROBO2 protein across species. Next, we tested the functional relevance of the RGD motif. For this test, we generated an RGD-to-RGA (D288A) substitution mutant via site-directed mutagenesis, as confirmed by DNA sequencing chromatograms (Fig. 3A). WT and mutant Ig3 fragments were tagged with 6×His epitopes, expressed in *E. coli*, and purified using immobilized metal affinity chromatography and a size exclusion purification strategy. Sample purity was confirmed as single bands at the corresponding molecular weight on a Coomassie Blue-stained SDS-PAGE gel (Fig. 3B). In a solid-phase binding assay, the WT Ig3 domain bound robustly to integrins αvβ1 and αvβ3, while the RGA mutant exhibited markedly diminished binding (Fig. 3C). Additional SPR analysis further confirmed strong affinity of WT ROBO1-Ig3 for αvβ1 ($K_D$ = 6.209 ± 0.264 × $10^{-10}$ M) and low affinities for αvβ3 ($K_D$ = 8.501 ± 0.794 × $10^{-7}$ M) (Fig. 3D). In contrast, the RGA mutation resulted in a dramatic ~240,000-fold reduction in αvβ1 binding and a ~33-fold decrease in αvβ3 interaction (Fig. 3D).

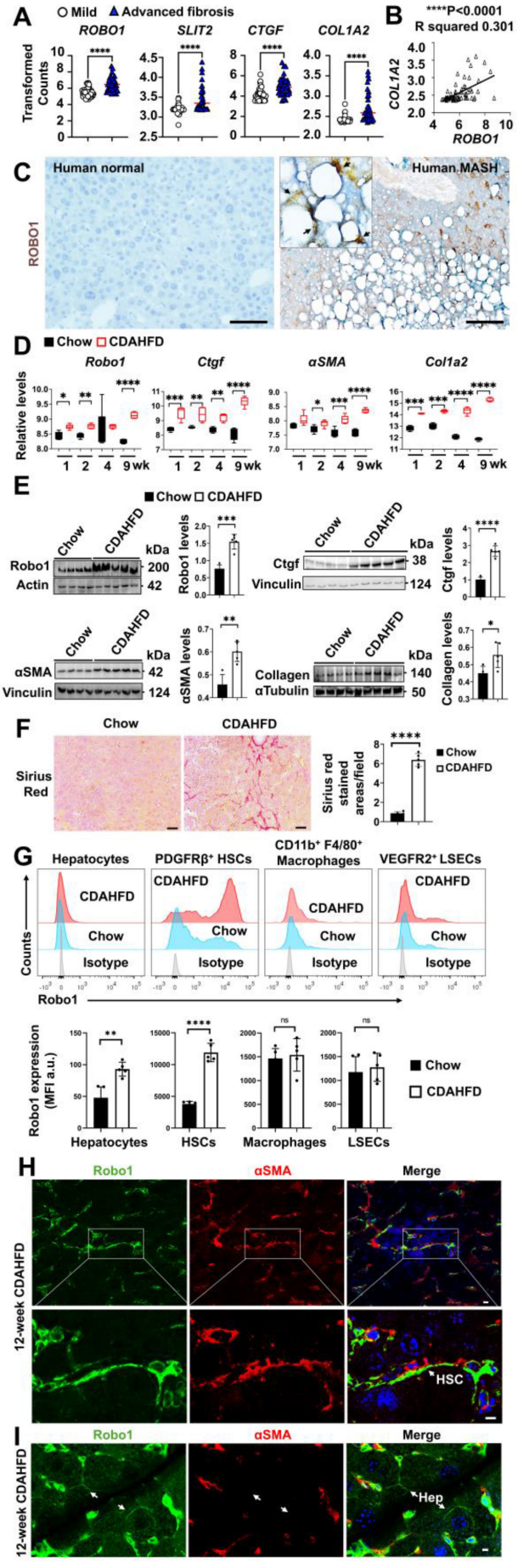



**Figure 1. ROBO1 is upregulated in human and experimental MASH and is associated with activated HSCs during liver fibrosis progression.** (A) show mRNA levels of *ROBO1*, *SLIT2* and fibrosis-associated genes (*CTGF* and *COL1A2*) in MASLD patients who suffered mild (fibrosis stages 0 and 1, n = 40) and advanced fibrosis (stages 3 and 4, n = 32). (B) A significant positive correlation was seen between *ROBO1* and *COL1A2* in these MASLD patients. Data in (A and B) were derived from a publicly available transcriptomic dataset GSE49541. (C) Immunohistochemistry on human liver sections revealed robust induction of ROBO1 in cells surrounding ballooning hepatocytes of MASH patients compared to normal controls. Scale bar: 100 μm. (D) *Robo1*, *Ctgf*, *αSMA*, and *Col1a2* transcripts were progressively upregulated in rat livers following CDAHFD feeding for 1, 2, 4, or 9 weeks (n = 5 per group) compared to age-matched chow-fed controls. Transcriptomic data were analyzed from GSE227714. (E) Western blotting and densitometric analyses for MASH livers post 12-week CDAHFD feeding in mice. Data were presented as mean ± SD from an unpaired *t*-test assuming normal distribution. Samples were derived from the same experiments but different gels for Ctgf and αSMA, with Vinculin as a loading control. Other loading controls included actin for Robo1 and α-tubulin for Collagen. Relative target protein expression was normalized to corresponding internal loading controls for each protein. (F) Sirius Red staining compared MASH-associated liver fibrosis between CDAHFD-fed mice and chow-fed controls. Scale bar: 50 μm. (G) Flow cytometry and quantitative analyses suggested higher levels of stained Robo1 protein, quantified by mean fluorescence intensity (MFI) in arbitrary units (a.u.), in primary hepatocytes and PDGFRβ$^+$ HSC, but not in CD45$^+$CD11b$^+$F4/80$^+$ macrophages and VEGFR2$^+$ LSEC of the 12-week CDAHFD-fed mice. (H and I) Immunofluorescent staining labeled Robo1 (green) on the surface of αSMA$^+$ HSCs (red) (H) and αSMA$^-$ hepatocytes (Hep) (I) in the 12-week CDAHFD-fed livers. Nuclei were stained with DAPI (blue). Scale bar: 10 μm. Data in (A, B, D-G) were represented as mean ± SD with $^*P < 0.05$, $^{**}P < 0.01$, $^{***}P < 0.001$, and $^{****}P < 0.0001$ (a two-sided unpaired Student's *t*-test).

RGD-containing integrins consist of 8 subtypes (αvβ1, αvβ3, αvβ5, αvβ6, αvβ8, α5β1, α8β1, and αIIbβ3) that are encoded by 9 genes (Supplementary Figure S4). Comparison of their expression patterns between early and advanced fibrosis in MASLD patients indicated little change of *ITGB6* (Genbank accession#AA609987), *ITGB8* (Genbank accession# BF513121), *ITGA2B* (Genbank accession#AF098114), *ITGB3* (Genbank accession#AI151479), and *ITGA5* (Genbank accession#NM_002205), while the other four genes were induced (Supplementary Figure S4). Notably, *ITGAV* (Genbank accession#AI093579) and *ITGB1* (Genbank accession#BG500301) that encode integrin αvβ1 protein were significantly upregulated in advanced MASLD group who had fibrosis stage 3 and 4 compared to early group (Fibrosis stage 0 and 1) (Fig. 3E). Moreover, *ITGAV* and *ITGB1* were positively correlated with induction of *ROBO1* in these clinical samples (Fig. 3F). Additional analyses of human patients showed significant inductions of *ITGAV* and *ITGB1* genes at both early MASLD and moderate MASH stages, whereas *SLIT2* and *ROBO1* were only significantly upregulated at moderate MASH (F3 stage) compared to healthy controls (Fig. 3G). These data indicate that the RGD motif within ROBO1's Ig3 domain is critical for integrin binding with a preferential interaction with αvβ1, suggesting a novel ligand-receptor axis that may contribute to fibrogenic signaling in MASH with fibrosis stages F3 and above.

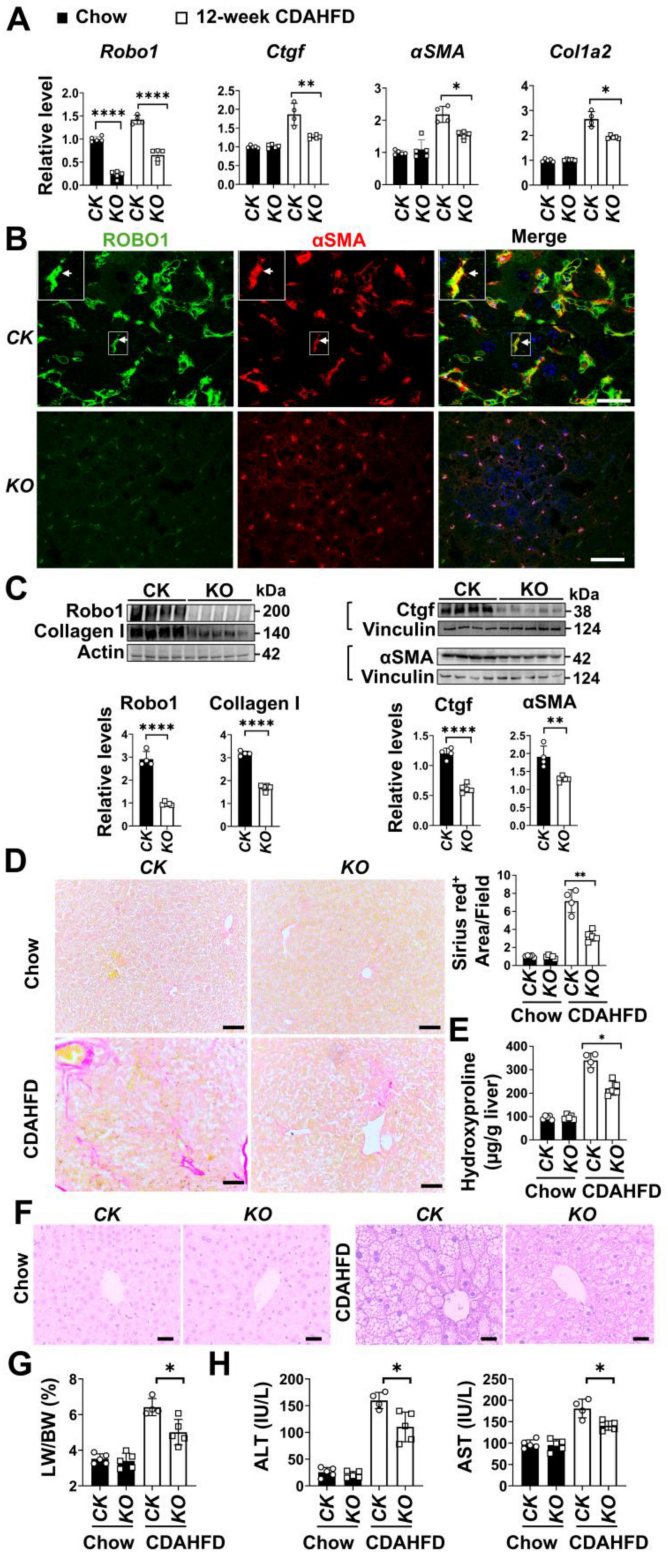



**Figure 2. HSC-specific deletion of the *Robo1* gene attenuates liver fibrosis in CDAHFD-fed mice.** (A) qRT-PCR analysis showed low induction of fibrotic genes in CDAHFD-fed HSC-specific *Robo1* knockouts (KO, driven by *Lrat-Cre*) compared to control littermates (CK) that were *Robo1* floxed homozygotes. Relative expression in these animals was normalized to chow-fed CK (n = 4-5 per group). (B) The immunofluorescent staining showed that Robo1 loss was associated with reduced staining of αSMA$^+$ HSCs, suggesting decreased HSC activation in the KO livers compared to CK after 12-week CDAHFD feeding. Robo1 (green), αSMA (red), and nuclei (blue) are shown. White arrows indicate αSMA$^+$Robo1$^+$ HSCs in higher-magnification images. Scale bar: 100 μm. (C) Western blotting and densitometric analysis detected lower levels of Robo1, type I collagen, Ctgf, and αSMA proteins in KO livers than CK at 12 weeks after CDAHFD feeding. Samples were analyzed on separate gels using the appropriate loading controls as follows: actin for Robo1 and Collagen, and vinculin for Ctgf and αSMA. Relative target protein expression was normalized to the corresponding internal loading control for each protein. (D) Sirius Red staining and quantification revealed reduced collagen deposition in the CDAHFD-fed KO livers compared to CK. Scale bar: 100 μm. (E) Hepatic hydroxyproline content was concomitantly decreased in the CDAHFD-fed KO livers compared to CK groups (n = 4-5 per group), indicating reduced production of hepatic collagen. (F) H&E staining of CK and KO livers of chow- and CDAHFD-fed mice. Scale bar: 100 μm. (G and H) CDAHFD feeding induced higher levels of liver to body weight ratios, serum ALT, and serum AST in CK groups (n = 4) than KO cohorts (n = 5), although no difference was found in the two groups that received the chow diet (n = 5 per group). Data in (A, C-E, G, and H) were expressed as mean ± SD with $^*P < 0.05$, $^{**}P < 0.01$, $^{**}P < 0.001$, and $^{****}P < 0.0001$ in a two-sided unpaired Student's t-test.

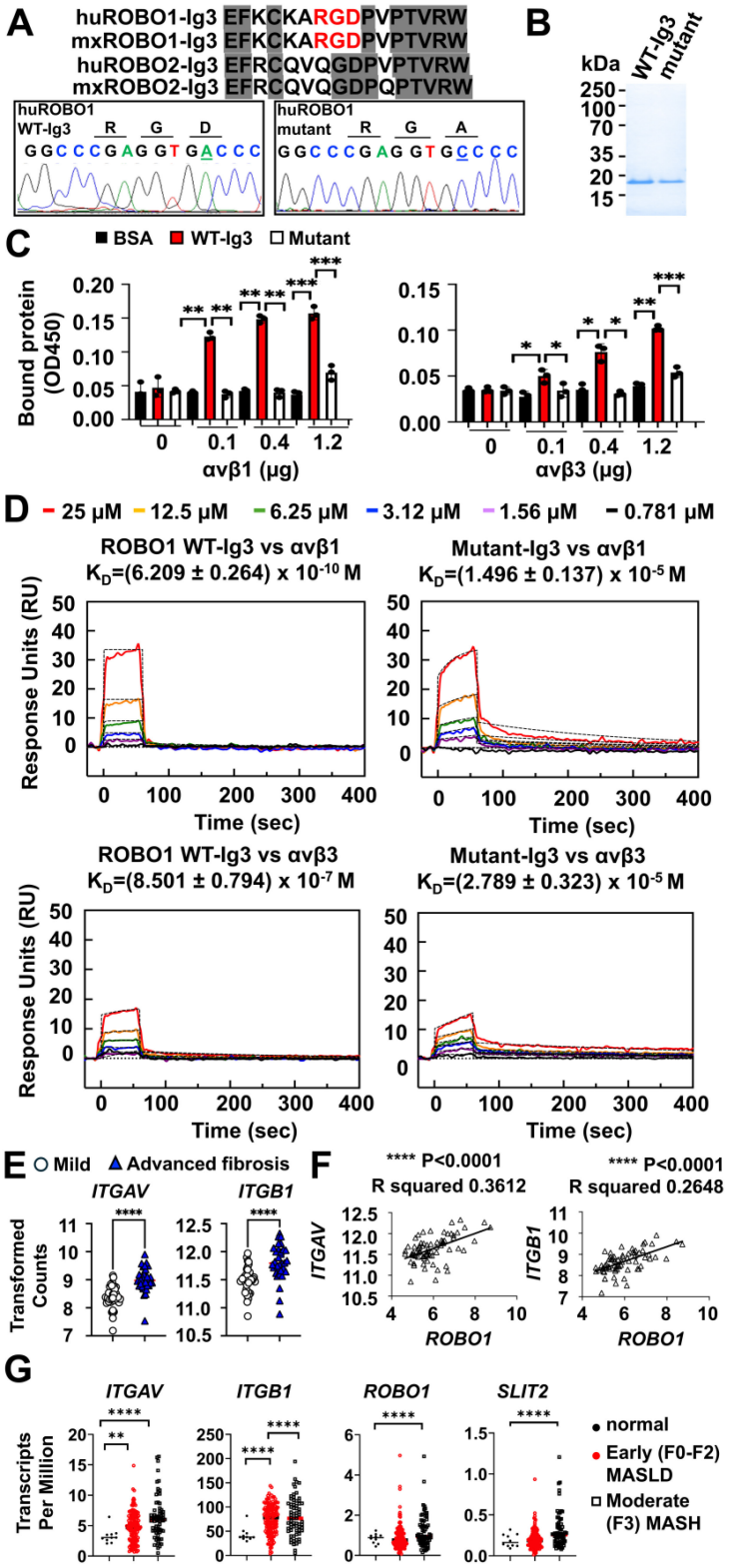



**Figure 3. The ROBO1 Ig3 domain contains an RGD motif that mediates high-affinity binding to integrin αvβ1.** (A) Sequence alignment of the Ig3 domain for human (hu) and mouse (mx) ROBO1 reveals the presence of an evolutionarily conserved RGD motif, which is absent in ROBO2. Sanger sequencing confirmed the successful generation of an RGA point mutation (D to A) in ROBO1-Ig3 using site-directed mutagenesis, with a nucleotide substitution from "A" to "C" as shown in chromatograms. (B) His tagged WT-Ig3 and mutant proteins were expressed in *E. coli* and purified using immobilized metal affinity chromatography and a size exclusion purification strategy. (C) Solid-phase binding assays demonstrated that the WT-Ig3 protein bound directly to recombinant human integrins αvβ1 and αvβ3 in a dose-dependent manner, whereas the RGA mutant lost this binding capacity. BSA served as a negative control. (D) SPR analysis of binding kinetics between integrins αvβ1 or αvβ3 and WT-Ig3 or RGA-mutant Ig3. (E and F) *ITGAV* and *ITGB1* were significantly induced (E) and were positively correlated with *ROBO1* expression in advanced-stage (n = 32) MASLD patients compared to early-stage MASLD controls (n = 40) (F). (G) *ITGAV* and *ITGB1* genes were not only induced in MASH livers (n = 138) but also MASLD with early liver fibrosis (F0-F2) (n = 68) in comparison to normal donors (n = 10), while *SLIT2* and *ROBO1* were only induced during MASH. Data were represented as mean ± SD, and were derived from a publicly available transcriptomic dataset GSE49541 in (E and F) and GSE135251 in (G). Values in (C, E-G) represent mean ± SD with $^{*}P < 0.05$, $^{**}P < 0.01$, $^{***}P < 0.001$, and $^{****}P < 0.0001$ (a two-sided unpaired Student's t-test).

### SLIT2 and CTGF potentiate RGD-dependent ROBO1 and integrin αvβ1 interaction and downstream profibrotic signaling

To investigate the role of the RGD motif in ROBO1 and integrin interaction, we engineered human LX-2 HSCs that stably expressed HA-tagged integrin αvβ1. The full-length ROBO1:V5 or mutant:V5 was transfected into these LX-2 HSCs. Two days later, recombinant SLIT2:Myc protein in combination with or without the FLAG-tagged CTGF protein was added to stimulate the transfected LX-2 cells. Parental LX-2 cells were transfected with the pLVX empty vector and used as negative controls in parallel studies. Pull-down assays using anti-V5 agarose revealed that integrin αvβ1 co-immunoprecipitated with ROBO1:V5 in the presence of SLIT2:Myc while these effects were not seen in cells that were transfected with empty vector or stimulated with Mock controls (Fig. 4A). The addition of CTGF:FLAG protein potentiated the SLIT2:Myc-stimulated receptor interactions, whereas RGA substitution in mutant:V5 caused loss of these activities (Fig. 4A), indicating RGD-dependent interaction.

ROBO1/integrin αvβ1 bindings were supported by PLA in which interactions brought plus and minus probes to close distances, leading to the generation of red fluorescent tagged products (Fig. 4B). This close physical interaction between these two receptors was lost in cells expressing the RGA mutant (Fig. 4B). Mechanistically, we investigated the downstream signaling pathway. Activation of the PI3K/AKT/β-Catenin axis was observed upon SLIT2 stimulation in ROBO1:V5-expressing LX-2 cells, and this activation was further amplified by CTGF co-treatment in comparison to empty vector controls (Fig. 4C). In contrast, expression of the RGA mutant markedly attenuated phosphorylation of PI3K, AKT, and β-Catenin at Ser552 (Fig. 4C), a modification known to promote the nuclear translocation and transcriptional activity of β-Catenin [30]. To rule out contamination by cytosolic β-catenin, we assessed the purity of the isolated nuclear fractions. Western blotting showed minimal signal for the cytoplasmic marker GAPDH, indicating negligible cytosolic contamination, while Ponceau S staining confirmed efficient transfer of nuclear proteins to the membranes (Fig. 4C). Consistent with this signaling attenuation by the RGA mutant, mRNA levels of canonical β-Catenin target genes (*aSMA* [31] and *Col1a2* [32]) were significantly upregulated in response to SLIT2/ROBO1 signaling, especially in the presence of CTGF. However, this upregulation was blunted in RGA mutant-expressing cells (Fig. 4D), confirming that the RGD-dependent ROBO1-integrin αvβ1 interaction is critical for pro-fibrotic gene induction. Notably, little difference between SLIT2:Myc+ROBO1:V5+αvβ1:HA and SLIT2:Myc+Mutant:V5+αvβ1:HA+CTGF: FLAG groups was observed (Fig. 4C and D), suggesting that CTGF alone is sufficient for activating PI3K, AKT, and β-Catenin signaling, even in the presence of mutated ROBO1. This observation is consistent with previous reports demonstrating that CTGF can directly activate PI3K, AKT, and β-Catenin pathways [17, 33]. Nevertheless, maximal activation of the PI3K/AKT/β-Catenin axis and the highest induction of *aSMA* and *COL1A2* were found upon co-stimulation with SLIT2:Myc and CTGF:FLAG in ROBO1:V5- and αvβ1:HA-expressing LX-2 cells (Fig. 4C and D), suggesting synergistic interactions between the CTGF/αvβ1 and SLIT2/ROBO1 pathways.

### Ectopic expression of ROBO1 ectodomains containing the RGD motif inhibits Akt/β-Catenin and TGF-β/Smad3 signaling in HSC of CDAHFD-fed mice

We previously demonstrated that the extracellular domains of the ROBO1 receptor in an Fc fusion chimera functioned as a ligand trap and suppressed SLIT2/ROBO1-mediated fibrotic signaling by interfering with CTGF crosstalk [17]. To examine the *in vivo* relevance of the RGD motif in ROBO1-integrin αvβ1 binding, we delivered AAV8 viruses expressing either WT ROBO1N:Fc or mutant:Fc in which the RGD motif was substituted with the RGA tripeptides into mice at the onset of 12-week CDAHFD feeding. AAV8-GFP was delivered in parallel as a control. PLA assays revealed robust interactions between endogenous ROBO1 and integrin αvβ1 in livers of AAV8-GFP and mutant:Fc-infected mice. In contrast, PLA signals were significantly reduced in AAV8-ROBO1N:Fc-infected livers, consistent with competitive blockade of endogenous ROBO1-integrin binding by the soluble ROBO1N:Fc decoy (Fig. 5A and B). Further co-immunoprecipitation with anti-human Fc beads pulled down integrin αvβ1 from total protein lysates of mouse HSCs that were isolated from ROBO1N:Fc-treated livers, confirming direct extracellular interaction *in vivo*. No such interactions were observed in HSCs from untreated mice or from mice treated with AAV8-GFP or AAV8-mutant:Fc (Fig. 5C). Functionally, AAV8-ROBO1N:Fc administration in these primary HSC isolated from CDAHFD-fed mice markedly attenuated the phosphorylation of Akt at Serine 473 and β-Catenin at Serine 552, as well as nuclear accumulation of β-Catenin and the active phosphorylated Smad3 in the TGF-β downstream signaling. The isolated nuclear fractions were highly

pure, with minimal contamination by the cytoplasmic marker Gapdh, and Ponceau S staining confirmed efficient transfer of nuclear proteins to the membranes (Fig. 5D). In contrast, the mutant lacking the RGD motif exhibited minimal antagonistic activity and continued to induce high levels of Akt/β-Catenin and TGF-β/Smad3 signaling (Fig. 5D and E). Together, these observations demonstrate the pathogenic role of ROBO1-integrin αvβ1 interactions in HSC activation.

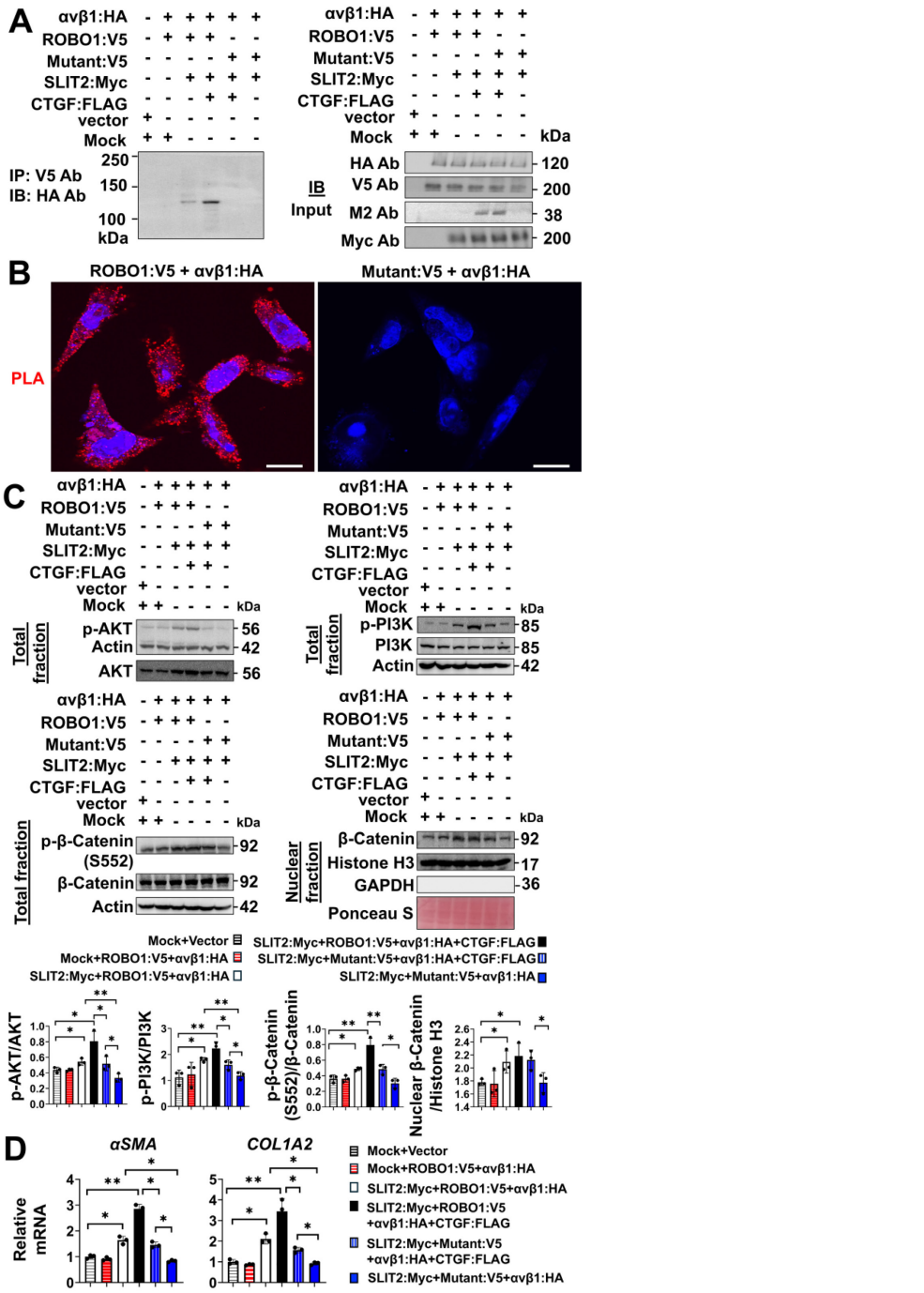



**Figure 4. SLIT2 and CTGF potentiate RGD-dependent ROBO1-integrin αvβ1 interaction and PI3K/AKT/β-Catenin signaling.** (A) Co-immunoprecipitation analysis showed that SLIT2 expression enabled ROBO1-integrin αvβ1 complex formation, which was further enhanced by CTGF. RGA mutation disrupted this ROBO1-integrin αvβ1 interaction. (B) PLA assays detected ROBO1-integrin αvβ1 complex formation (red signals) in LX-2 HSCs that were stimulated with SLIT2:Myc and CTGF:FLAG proteins. These complexes were not detected in cells expressing the RGA mutation. Nuclei were counterstained with DAPI (blue). Scale bar: 20 μm. (C) Immunoblotting examined levels of p-PI3K, PI3K, p-β-Catenin (S552), β-Catenin, p-AKT, and AKT proteins in total liver lysates or nuclear fractions of LX-2 cells that expressed integrin αvβ1:HA and ROBO1:V5 after stimulation by Mock, SLIT2:Myc, or/and CTGF:FLAG. Notably, RGA mutation caused reduced phosphorylation of these signaling molecules. Samples were analyzed using actin and Histone H3 as loading controls. Nuclear extracts were also probed for GAPDH to rule out cytosolic contamination while Ponceau S staining was used to verify nuclear protein loading. Relative target protein expression was quantified in densitometric analyses and normalized to the corresponding internal loading control for each protein. (D) qRT-PCR analysis demonstrated upregulation of fibrosis-related genes (*αSMA* and *COL1A2*) in LX-2 cells that were stimulated by SLIT2:Myc or/and CTGF:FLAG, whereas RGA mutation significantly impaired these inductions. Data in (C and D) were mean ± SD with $^{*}P < 0.05$ and $^{**}P < 0.01$ in two-sided unpaired Student's t-test.

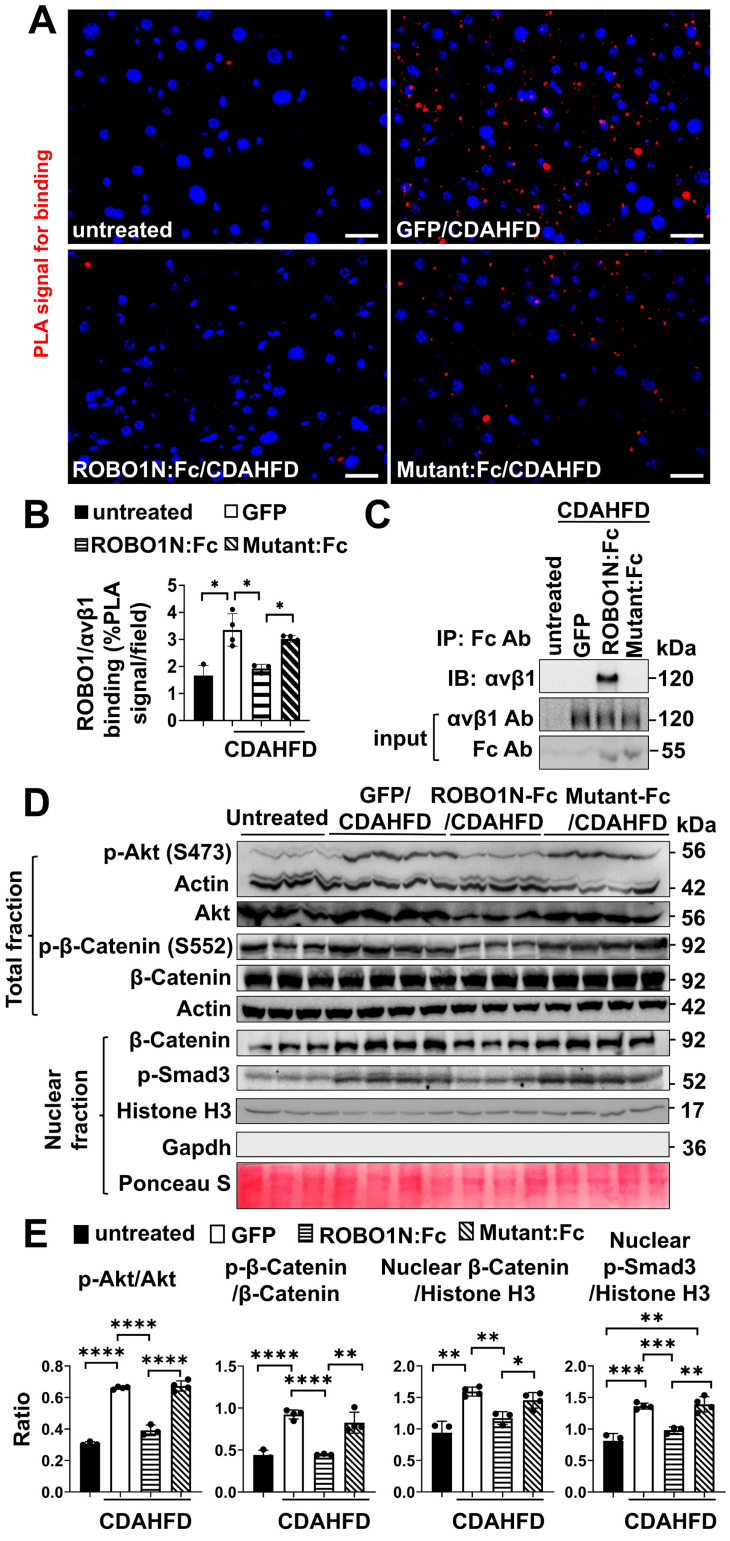



**Figure 5. ROBO1N:Fc disrupts ROBO1-integrin αvβ1 interaction and inhibits Akt/β-Catenin and TGF-β/Smad3 signaling in HSCs from CDAHFD-fed mice.** (A and B) ROBO1-αvβ1 binding was indicated by red signals in PLA assays (A) and quantification (B) from untreated or CDAHFD-fed mice that were infected with AAV8-GFP, AAV8-ROBO1N:Fc, or AAV8-mutant:Fc. Scale bar: 50 μm. (C) Co-immunoprecipitation assays revealed that ROBO1N:Fc, but not the RGA mutant, efficiently pulled down integrin αvβ1 from primary HSC of CDAHFD-fed mice. Protein extracts were incubated with anti-human Fc-conjugated beads. Bound proteins were immunoblotted with integrin αvβ1 or Fc antibodies. Input confirmed equivalent protein loading. (D and E) Immunoblotting (D) and densitometric analyses (E) showed inhibition of Akt/β-Catenin and TGF-β/Smad3 signaling by ROBO1N:Fc in CDAHFD-fed livers (n = 3), whereas this antagonistic activity was lost in the RGA mutant:Fc (n = 4) in comparison to the untreated group (n = 3) and GFP/CDAHFD-fed group (n = 4). Samples were immunoblotted with loading controls (actin and Histone H3). Gapdh was stained to rule out cytosolic contamination in nuclear extracts. Ponceau S was also used to verify nuclear protein loading. Relative expression of tested proteins was normalized to their corresponding internal loading controls. Data in (B and E) were calculated in the indicated animal groups (n = 3 to 4 per group). Values are mean ± SD with $^{*}P < 0.05$, $^{**}P < 0.01$, $^{***}P < 0.001$, and $^{****}P < 0.0001$ in a two-sided unpaired Student's *t*-test.

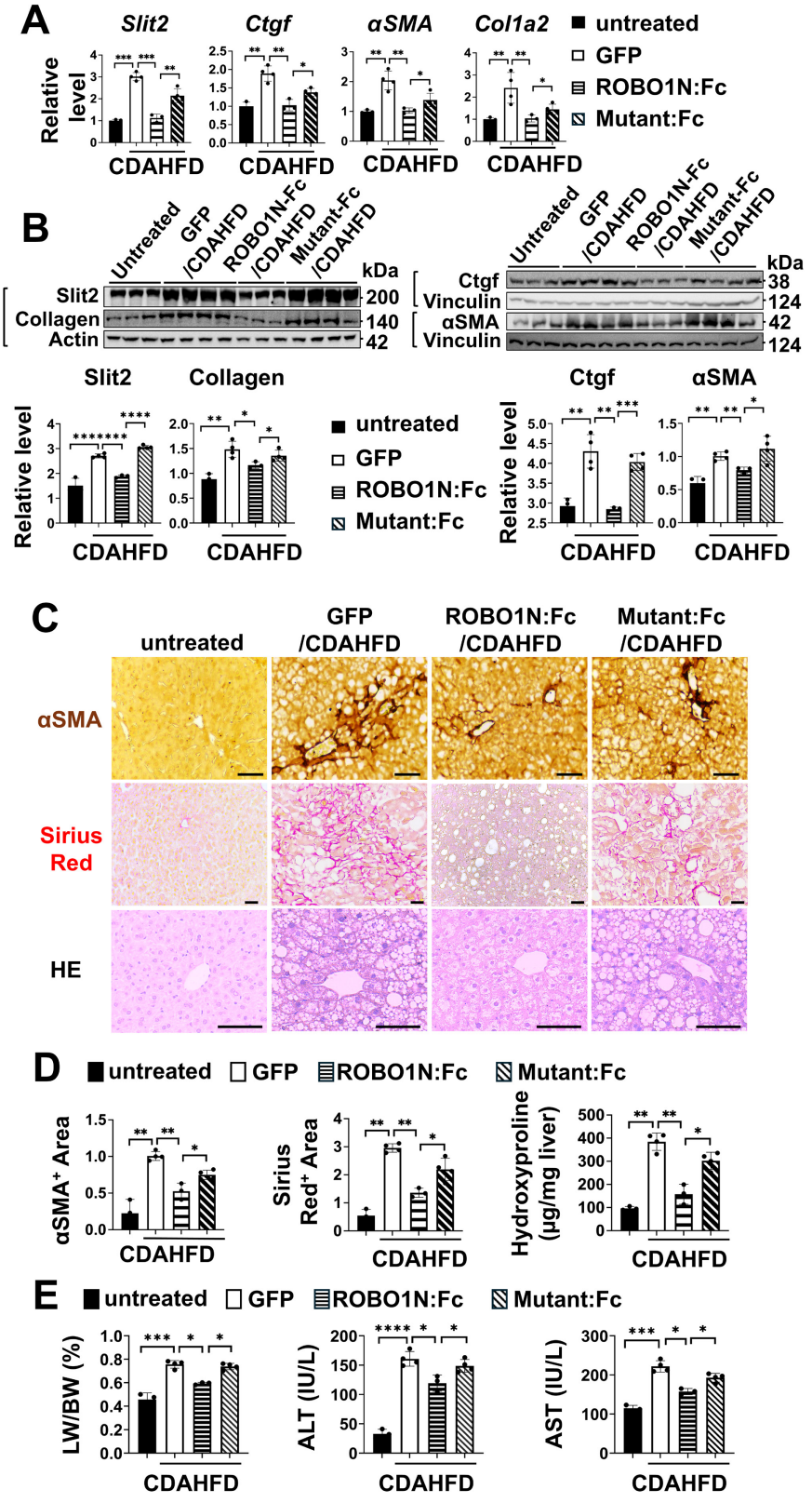



**Figure 6. AAV8-mediated ROBO1N:Fc delivery inhibits CDAHFD-induced liver fibrosis in an RGD-dependent manner.** (A) qRT-PCR analyses were quantified from untreated (n = 3) and 12-week CDAHFD-fed livers from animals infected with AAV8-GFP (n = 4), ROBO1N:Fc (n = 3), and RGA mutant:Fc (n = 4). (B) shows immunoblotting and densitometric quantification. Samples were derived from the same experiments but run on separate gels using the appropriate loading controls: actin for Slit2 and Collagen, and vinculin for Ctgf and αSMA. Relative target protein expression was normalized to these corresponding loading controls. (C) are representative images of H&E staining, αSMA staining, and Sirius Red staining. Scale bar: 100 μm. (D) shows quantification of αSMA⁺ areas, Sirius Red⁺ areas, and hepatic hydroxyproline content for the indicated groups. (E) shows graphs for liver-to-body weight ratios and serum levels of ALT and AST. Data in (A, B, D, and E) were mean ± SD with $^{*}P < 0.05$, $^{**}P < 0.01$, $^{***}P < 0.001$, and $^{****}P < 0.0001$ (two-sided unpaired Student's *t*-test).

### Ectopic expression of ROBO1 ectodomains attenuates CDAHFD-induced liver fibrosis in an RGD-dependent manner

To assess the therapeutic impact of ROBO1-integrin disruption on liver fibrosis in MASH, we examined fibrosis-related genes in the livers of mice treated with AAV8-ROBO1N:Fc containing the RGD motif or the RGA mutant after 12-week feeding of the CDAHFD diet. The qRT-PCR analysis revealed that AAV8-ROBO1N:Fc significantly reduced expression of *Ctgf, Slit2, aSMA,* and *Col1a2*, compared with AAV8-GFP controls. The RGA mutant exhibited mild suppression, indicating that the RGD motif is critical for full antifibrotic activity in AAV8-ROBO1N:Fc (Fig. 6A). Consistent with the transcriptional data, immunoblotting and densitometric quantification showed lower protein levels of Ctgf, Slit2, αSMA, and collagen proteins in the AAV8-ROBO1N:Fc group relative to AAV8-mutant:Fc, and AAV8-GFP-treated mice (Fig. 6B). Histological analyses further supported these findings, as H&E, αSMA, and Sirius Red staining demonstrated reduced hepatocyte ballooning, myofibroblast activation, and collagen deposition in ROBO1N:Fc-treated livers (Fig. 6C). Morphometric quantification confirmed a marked reduction in $\alpha SMA^+$ areas, Sirius Red-stained areas, and hepatic hydroxyproline content in the AAV8-ROBO1N:Fc group compared to AAV8-GFP and AAV8-mutant:Fc groups (Fig. 6D). Accordingly, decreases in liver-to-body weight ratio and reduced levels of ALT and AST in sera were seen in the AAV8-ROBO1N:Fc-treated group (Fig. 6E). Together, these results suggest that ROBO1 ectodomains carrying an intact RGD motif potently suppress MASH-associated liver fibrosis *in vivo*. The diminished efficacy of the RGA mutant underscores the essential role of RGD-mediated integrin engagement in driving fibrotic signaling.

## Discussion

MASLD encompasses a spectrum of liver pathology from benign steatosis to the more aggressive MASH, characterized by chronic inflammation and progressive fibrogenesis. This study provides the first evidence about the critical roles of the SLIT2/ROBO1 signaling in MASH-associated liver fibrosis. In patients with MASH, liver fibrosis is the main determinant of mortality. While early-stage fibrosis may still be reversible, the transition to advanced stages-particularly cirrhosis-is typically irreversible, ultimately resulting in organ failure and increased mortality. Given that liver fibrosis is a sustained inflammatory process driven by the activation and migration of HSCs and immune cells, the spatial expression pattern of Robo1 and its HSC-specific loss in this study suggest functional relevance of this receptor in this setting. The selective upregulation of Robo1 in mouse hepatocytes and HSCs reinforces its functional specificity in the pathogenesis of liver fibrosis induced by CDAHFD. The involvement of this axon guidance receptor, Robo1, points to an intriguing paradigm in organ fibrosis: the repurposing of neurodevelopmental pathways in adult mesenchymal cells. Neuroectodermal features may predispose HSCs to reactivate signaling modules such as Slit2-Robo1, which originally evolved to control neuronal migration and axon repulsion, during the CDAHFD-induced MASH.

ROBO1 was originally identified as a homophilic binding molecule regulating axonal pathfinding in response to stimulation by SLIT ligands [34]. Later, the functions of the SLIT/ROBO pathway have been extended to a diverse variety of pathological processes, including angiogenesis, tissue repair, and cancer development. In normal human livers, basal levels of *ROBO1* and *SLIT2* are found in hepatocytes, vascular endothelial cells, fibroblasts, Kupffer cells, smooth muscle cells, B cells, and macrophages, whereas ROBO1 protein is overexpressed in human HCC [15, 35-37]. ROBO1 has been shown to counteract suppression of HCC proliferation [36]. A ROBO1-neutralizing antibody can inhibit HCC growth and angiogenesis in animal models [38]. In addition, the SLIT2 protein is encoded by one of the liver immune microenvironment-related hub genes in biliary atresia, and its elevation has been found in the serum of patients with primary biliary cirrhosis [18, 20]. Upregulation of this ligand enhances liver susceptibility to injury induced by bile duct ligation, while its deletion reduces biliary fibrosis [20]. Moreover, SLIT2 can signal through ROBO receptors to promote liver fibrosis in experimental models induced by carbon tetrachloride, thioacetamide, or 3,5-diethoxycarbonyl-1,4-dihydrocollidin [16, 19]. The action mediated by the SLIT/ROBO signaling has been known to crosstalk with other pathways and induce fibrosis-related genes. The SLIT/ROBO signaling interferes with the TGF-β1/Smad pathway and upregulates Periostin synthesis during cardiac fibrosis [39]. By activating downstream molecules, this SLIT/ROBO signaling enhances phosphorylation of PI3K and AKT in liver and cardiac fibrosis [16, 39]. Moreover, it influences the phosphorylation status, localization, and function of intracellular effectors such as β-Catenin. This SLIT2/ROBO1 interaction likely impacts cell activation, adhesion, and migration [40, 41]. For instance, ROBO1 promotes the activation of Src and β-Catenin during intestinal tumorigenesis [42]. Src can act upstream of the PI3K and AKT

signaling [43]. AKT is known to phosphorylate β-Catenin at serine residue 552, leading to translocation of this transcriptional regulator into the nucleus [44]. β-Catenin is overexpressed in liver fibrosis, and its downregulation can inhibit HSC activation [45]. In this study, we identified a noncanonical activation of β-Catenin by the SLIT2/ROBO1/AKT signaling, which ultimately induced profibrotic signals (e.g., p-Smad3, αSMA, and COL1A2) in HSC. These findings provide new insights into the mechanisms underlying HSC activation in MASH.

Recent advances in crystal structural biology have provided critical insights into the conformational dynamics of ROBO1, revealing that it typically resides in a tetrameric, auto-inhibited configuration stabilized through "back-to-back" interactions involving its central Ig-like domains [46]. The binding of its canonical ligand, SLIT2, to the Ig1–Ig2 tandem induces a pronounced conformational rearrangement that exposes previously concealed motifs and converts ROBO1 into its active, signaling-competent form. Within this context, our study identified a conserved RGD motif embedded in the Ig3 domain of ROBO1 as a structurally regulated functional site. Consistent with structural predictions, our data support a model in which SLIT2-mediated ROBO1 activation promotes accessibility or productive engagement of the Ig3 RGD motif. Given that the central Ig domains (Ig3-Ig4) of ROBO1 are buried in the inactive "back-to-back" tetrameric assembly[46], the RGD site in Ig3 likely becomes surface-exposed only upon activation with functional signaling outputs, triggering integrin engagement via tightly coupled ligand-induced conformational changes. Importantly, we established a mechanistic link between this interaction and liver fibrosis by demonstrating that the RGD motif is indispensable for ROBO1-mediated activation of HSCs and mediates a functionally specific interaction between ROBO1 and integrin αvβ1 receptors (Fig. 7). Our findings extend this functional repertoire by showing that αvβ1 directly binds to the RGD motif within the Ig3 domain of ROBO1. This interaction was observed under both *in vitro* and *in vivo* conditions and was shown to be critical for ROBO1-mediated activation of HSCs. Disruption of this RGD motif through point mutation (RGA substitution) abolished ROBO1-αvβ1 binding. The RGA mutation attenuated the fibrogenic response, as demonstrated by reduced HSC activation and collagen deposition in CDAHFD-fed mice treated with the mutant ROBO1N:Fc construct. Importantly, the antifibrotic efficacy of ROBO1N:Fc chimera, achieved via AAV8-mediated gene transfer, was significantly lost when the RGD motif was mutated. This not only highlights the functional indispensability of the RGD sequence for integrin binding but also underscores the specificity of the ROBO1-αvβ1 axis in mediating HSC activation during MASH progression.

ROBO1 represents a high-affinity αvβ1-binding partner in the context of liver fibrosis compared to αvβ3, although we cannot rule out additional interactions between this receptor and other RGD-binding integrins. We propose that this specificity arises from a higher-order molecular complex that comprises SLIT2, ROBO1, CTGF, and integrin αvβ1 as a macromolecular signaling complex. Activation of the Integrin αv/CTGF axis via Yes-associated protein (YAP) has been reported to promote liver fibrogenesis, leading to portal hypertension and liver carcinogenesis in congestive hepatopathy [47]. We speculate that CTGF and integrin αvβ1 contribute to the initiation of liver fibrosis during MASLD progression, given their established role in TGF-β activation [48, 49]. Supporting this notion, analysis of publicly available datasets (GSE49541 and GSE135251) revealed significant induction of *ITGAV* and *ITGB1* expression at early MASLD as well as advanced MASH stages, whereas *SLIT2* and *ROBO1* expression was not elevated until moderate MASH with liver fibrosis stages at F3 or higher in this study. These differential expression patterns suggest that the CTGF/integrin αvβ1 pathway may drive early fibrotic responses in MASLD, while SLIT2/ROBO1 signaling, induced later in MASH, synergizes to exacerbate fibrosis. This late induction of the SLIT2/ROBO1 pathway may be controlled transcriptionally by antifibrotic regulators, such as LIM Homeobox 2 (LHX2), which is a known inhibitor of ROBO1 in neuronal development and plays a key role in the inhibition of liver fibrosis [50, 51]. Considering that LHX2 is often downregulated in MASH [51], loss of this transcriptional repressor likely contributes to ROBO1 induction. SLIT2 binds to ROBO1 and promotes its conformational activation. Within this configuration, the RGD motif of ROBO1 becomes accessible, allowing productive interaction with αvβ1, and ultimately amplifying HSC activation. In addition, CTGF can potentiate ROBO1 signaling via its ability to interact with both integrin αvβ1 and SLIT2 [17, 52]. This modular cooperation provides a molecular explanation for the observed synergy between SLIT2-ROBO1 signaling and integrin-driven fibrogenesis, positioning this axis as a central conduit linking inflammation, mechanotransduction, and ECM remodeling in MASH. The elegance of this modular interaction lies not only in its structural specificity but also in its biological precision. Integrin αvβ1 is known to participate in a range of cellular processes. Yet, our findings highlight that its fibrogenic engagement starts in early fibrosis during MASLD, and can be

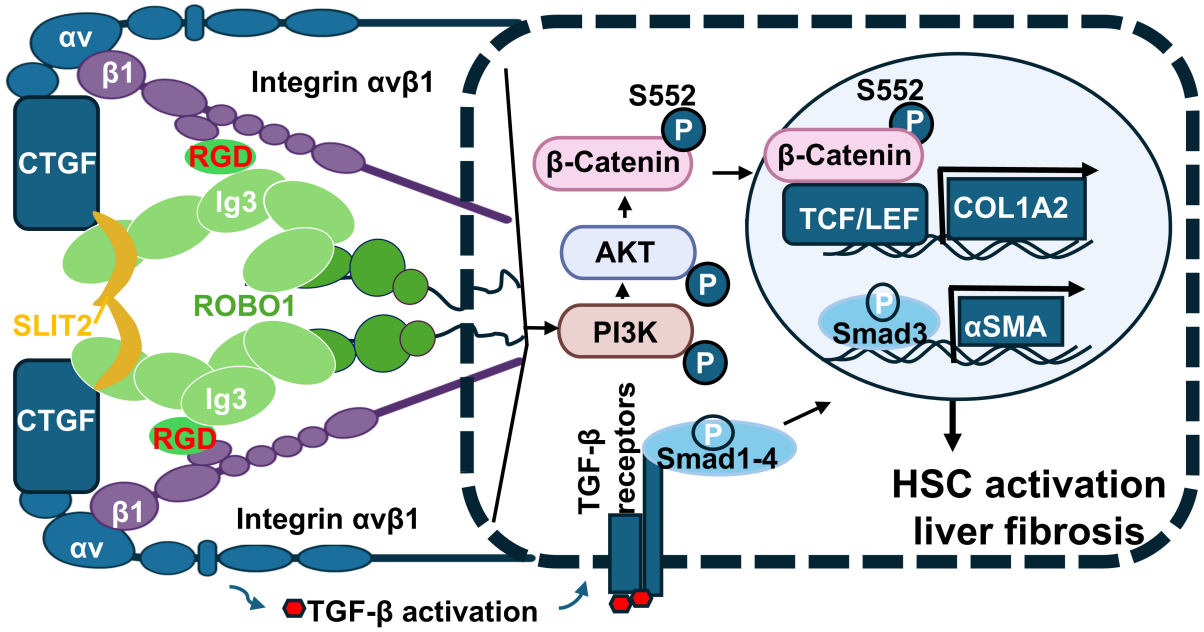



**Figure 7. Proposed model for RGD-dependent ROBO1-integrin αvβ1 signaling in MASH-associated liver fibrosis.** Our data suggest that concurrent engagement of CTGF and SLIT2 promotes the assembly of a ROBO1-integrin αvβ1 receptor complex, potentially stabilized through recognition of the RGD motif within the ROBO1 Ig3 domain by integrin αvβ1. SLIT2 binds to the Ig1-Ig2 domains of ROBO1, whereas CTGF functions as a ligand for integrin αvβ1, a known activator of TGF-β signaling. In addition, CTGF can directly interact with SLIT2 to further potentiate ROBO1 signaling. Co-activation of these ligand/receptor complexes synergistically enhances downstream signaling pathways, leading to phosphorylation of Smad3, PI3K, AKT, and β-catenin at Ser552. Activated β-catenin and phosphorylated Smad3 subsequently translocate into the nucleus, where they induce profibrotic target genes, including αSMA and COL1A2, thereby driving CDAHFD-induced MASH-associated liver fibrosis.

contextually synergized by ROBO1 activation in MASH, thereby conferring a layer of signal fidelity unique to HSCs. These findings hold broad implications: the SLIT2/ROBO1/CTGF/αvβ1 axis constitutes a unique fibrogenic circuit that is selectively operative in neural crest-derived mesenchymal cells such as HSCs. Its modularity, receptor specificity, and activation dependency render ROBO1 an attractive therapeutic target for anti-fibrotic intervention, potentially enabling precise disruption of disease-driving pathways while sparing homeostatic functions in MASH. We speculate that ROBO1 may play a conserved pro-fibrotic role across other forms of chronic liver disease. For example, HSCs are activated in alcohol-associated liver disease (ALD) and metabolic dysfunction-associated ALD (MetALD) [53, 54]. SLIT2 and ROBO1 are heavily upregulated in advanced ALD and linked with ductular reaction and abnormal blood vessel growth [19]. Moreover, CTGF mediates ethanol-stimulated differentiated functions of human and mouse HSCs [55]. Collectively, these findings raise the possibility that targeting the SLIT2/ROBO1/CTGF/αvβ1 axis could attenuate liver fibrosis in ALD and MetALD.

In summary, our data suggest that the ROBO1-integrin αvβ1 interaction, mediated by the RGD motif, actively promotes fibrotic signaling in MASH. The soluble ectodomain of ROBO1 acts not only as a functional antagonist of HSC activation but also as a novel therapeutic scaffold. Its design principles, based on structural biology, motif-specificity, and *in vivo* efficacy, lay the foundation for a new class of biologics tailored to target ECM-linked fibrogenic circuits in MASH and potentially other solid organ fibroses. Further refinement and optimization of this strategy could enable the development of decoy-based therapeutics with improved delivery, minimal toxicity, and enhanced tissue specificity.

## Abbreviations

ROBO: roundabout; Ig: immunoglobulin; MASH: metabolic dysfunction-associated steatohepatitis; CDAHFD: choline-deficient, high-fat, L-amino acid–defined high fat diet; HSC: hepatic stellate cells; RGD: arginine-glycine-aspartic acid; RGA: arginine-glycine-alanine; AAV8: adeno-associated virus 8; SLIT2: slit guidance ligand 2; CTGF: connective tissue growth factor; PI3K: phosphatidylinositol 3-kinase; AKT: protein kinase B; MASLD: Metabolic dysfunction-associated steatotic liver disease; NASH: nonalcoholic steatohepatitis; HCC: hepatocellular carcinoma; ECM: extracellular matrix; FDA: food and drug administration; GLP-1: glucagon-like peptide-1; GIPR: glucose-dependent insulinotropic polypeptide receptor; TGF: transforming growth factor; Lrat: lecithin: retinol acyltransferase; CBA: chicken β-actin; RT-PCR: reverse transcriptase-polymerase chain reaction; αSMA: α smooth muscle actin; TBS: Tris-

buffered saline; BSA: bovine serum albumin; HRP: horseradish peroxidase; SPR: surface plasmon resonance; FBS: fetal bovine serum; PLA: proximity ligation assay; KO: knockout; Fn: fibronectin; TAA: thioacetamide; DDC: 3,5-diethoxycarbonyl-1,4-dihydrocollidine; CK: control; PVDF: polyvinylidene difluoride.

## Supplementary Material

Supplementary figures.
https://www.ijbs.com/v23p0001s1.pdf

## Acknowledgments

This study is supported by the National Institutes of Health NIAAA R01AA028035, R01AA03523, NIDDK R01DK149400 grant and the Lavin Bernick Grant Funding awarded to L.P. In addition, H.L. was in part supported by U01CA252964, the Ladies Leukemia League Foundation, the Krewe de Pink Foundation, and the Reynolds and Ryan Families Endowed Chair fund.

### Data availability statements

All data supporting the findings of this study are available within the paper and within its supplementary materials published online.

### Author contributions

T Tian, M Nzegwu, A Mrozek, Y Xue, R Tandra, H Lu, H Park, and L Pi designed research. T Tian, M Nzegwu, A Mrozek, A Zhirkova, M Mannan, CB Sun, and L Pi performed experiments and analyzed data. T Tian, M Nzegwu, A Mrozek, Y Xue, L Pi wrote the article. All authors read a draft of this article, suggested improvements, and approved the final version.

## Competing Interests

The authors have declared that no competing interest exists.

## References

1. Horn P, Tacke F. Key takeaways from the updated multidisciplinary European MASLD guidelines. eGastroenterology. 2025;3:e100196.
2. Yang Z, Liu Z, Liu W, et al. Steatotic liver disease and cancer: from pathogenesis to therapeutic targets. eGastroenterology. 2025;3:e100218.
3. European Association for the Study of the L, European Association for the Study of D, European Association for the Study of O. EASL-EASD-EASO Clinical Practice Guidelines on the management of metabolic dysfunction-associated steatotic liver disease (MASLD). J Hepatol. 2024;81:492-542.
4. Jara M, Norlin J, Kjaer MS, et al. Modulation of metabolic, inflammatory and fibrotic pathways by semaglutide in metabolic dysfunction-associated steatohepatitis. Nat Med. 2025;31:3128-3140.
5. Sanyal AJ, Bedossa P, Fraessdorf M, et al. A Phase 2 Randomized Trial of Survodutide in MASH and Fibrosis. N Engl J Med. 2024;391:311-319.
6. Loomba R, Hartman ML, Lawitz EJ, et al. Tirzepatide for Metabolic Dysfunction-Associated Steatohepatitis with Liver Fibrosis. N Engl J Med. 2024;391:299-310.
7. Ludwig BS, Kessler H, Kossatz S, et al. RGD-Binding Integrins Revisited: How Recently Discovered Functions and Novel Synthetic Ligands (Re-)Shape an Ever-Evolving Field. Cancers (Basel). 2021;13:1711.
8. Slack RJ, Macdonald SJF, Roper JA, et al. Emerging therapeutic opportunities for integrin inhibitors. Nat Rev Drug Discov. 2022;21:60-78.
9. Reed NI, Jo H, Chen C, et al. The alphavbeta1 integrin plays a critical *in vivo* role in tissue fibrosis. Sci Transl Med. 2015;7:288ra79.
10. Wilkinson AL, Barrett JW, Slack RJ. Pharmacological characterisation of a tool alphavbeta1 integrin small molecule RGD-mimetic inhibitor. Eur J Pharmacol. 2019;842:239-247.
11. Henderson NC, Arnold TD, Katamura Y, et al. Targeting of alphav integrin identifies a core molecular pathway that regulates fibrosis in several organs. Nat Med. 2013;19:1617-24.
12. Kidd T, Brose K, Mitchell KJ, et al. Roundabout controls axon crossing of the CNS midline and defines a novel subfamily of evolutionarily conserved guidance receptors. Cell. 1998;92:205-15.
13. Brose K, Bland KS, Wang KH, et al. Slit proteins bind Robo receptors and have an evolutionarily conserved role in repulsive axon guidance. Cell. 1999;96:795-806.
14. Wu JY, Feng L, Park HT, et al. The neuronal repellent Slit inhibits leukocyte chemotaxis induced by chemotactic factors. Nature. 2001;410:948-52.
15. Basha S, Jin-Smith B, Sun C, et al. The SLIT/ROBO Pathway in Liver Fibrosis and Cancer. Biomolecules. 2023;13.
16. Chang J, Lan T, Li C, et al. Activation of Slit2-Robo1 signaling promotes liver fibrosis. J Hepatol. 2015;63:1413-20.
17. Pi L, Sun C, Jn-Simon N, et al. CCN2/CTGF promotes liver fibrosis through crosstalk with the Slit2/Robo signaling. J Cell Commun Signal. 2023;17:137-150.
18. Zhang J, Luo Y, Feng M, et al. Identification of Liver Immune Microenvironment-Related Hub Genes in Liver of Biliary Atresia. Front Pediatr. 2021;9:786422.
19. Coll M, Arino S, Martinez-Sanchez C, et al. Ductular reaction promotes intrahepatic angiogenesis through Slit2-Roundabout 1 signaling. Hepatology. 2022;75:353-368.
20. Li C, Yang G, Lin L, et al. Slit2 signaling contributes to cholestatic fibrosis in mice by activation of hepatic stellate cells. Exp Cell Res. 2019;385:111626.
21. Honey Hendesi, Mary F Barbe, Fayez F Safadi, et al. Integrin mediated adhesion of osteoblasts to connective tissue growth factor (CTGF/CCN2) induces cytoskeleton reorganization and cell differentiation. PLoS One. 2015;10:e0115325.
22. Runping Gao, Brigstock DR. Connective tissue growth factor (CCN2) induces adhesion of rat activated hepatic stellate cells by binding of its C-terminal domain to integrin alpha(v)beta(3) and heparan sulfate proteoglycan. J Biol Chem. 2004; 279:8848-55.
23. Matsumoto M, Hada N, Sakamaki Y, et al. An improved mouse model that rapidly develops fibrosis in non-alcoholic steatohepatitis. Int J Exp Pathol. 2013;94:93-103.
24. Zhou J, Sun C, Yang L, et al. Liver regeneration and ethanol detoxification: A new link in YAP regulation of ALDH1A1 during alcohol-related hepatocyte damage. FASEB J. 2022;36:e22224.
25. Pi L, Robinson PM, Jorgensen M, et al. Connective tissue growth factor and integrin alphavbeta6: a new pair of regulators critical for ductular reaction and biliary fibrosis in mice. Hepatology. 2015;61:678-91.
26. Pi L, Ding X, Jorgensen M, et al. Connective tissue growth factor with a novel fibronectin binding site promotes cell adhesion and migration during rat oval cell activation. Hepatology. 2008;47:996-1004.
27. Sun C, Fan W, Basha S, et al. Extracellular matrix protein 1 binds to connective tissue growth factor against liver fibrosis and ductular reaction. Hepatol Commun. 2024;8.
28. Varghese F, Bukhari AB, Malhotra R, et al. IHC Profiler: an open source plugin for the quantitative evaluation and automated scoring of immunohistochemistry images of human tissue samples. PLoS One. 2014;9:e96801.
29. Elvevold K, Kyrrestad I, Smedsrød B. Protocol for isolation and culture of Mouse hepatocytes (Hcs), Kupffer cells (KCs), and liver sinusoidal endothelial cells (Lsecs) in analyses of hepatic drug distribution. Methods Mol Biol. 2022;2434:385-402.
30. Fang D, Hawke D, Zheng Y, et al. Phosphorylation of beta-catenin by AKT promotes beta-catenin transcriptional activity. J Biol Chem. 2007;282:11221-9.
31. Charbonney E, Speight P, Masszi A, et al. beta-catenin and Smad3 regulate the activity and stability of myocardin-related transcription factor during epithelial-myofibroblast transition. Mol Biol Cell. 2011;22:4472-85.
32. Roh MR, Kumar R, Rajadurai A, et al. Beta-catenin causes fibrotic changes in the extracellular matrix via upregulation of collagen I transcription. Br J Dermatol. 2017;177:312-315.
33. Deng YZ, Chen PP, Wang Y, et al. Connective tissue growth factor is overexpressed in esophageal squamous cell carcinoma and promotes tumorigenicity through beta-catenin-T-cell factor/Lef signaling. J Biol Chem. 2007;282:36571-81.
34. Hivert B, Liu Z, Chuang CY, et al. Robo1 and Robo2 are homophilic binding molecules that promote axonal growth. Mol Cell Neurosci. 2002;21:534-45.
35. Avci ME, Konu O, Yagci T. Quantification of SLIT-ROBO transcripts in hepatocellular carcinoma reveals two groups of genes with coordinate expression. BMC Cancer. 2008;8:392.
36. Wang J, Zhou Y, Fei X, et al. Integrative bioinformatics analysis identifies ROBO1 as a potential therapeutic target modified by miR-218 in hepatocellular carcinoma. Oncotarget. 2017;8:61327-61337.

37. Pourhamzeh M, Asadian S, Mirzaei H, et al. Novel antigens for targeted radioimmunotherapy in hepatocellular carcinoma. Mol Cell Biochem. 2023;478:23-37.
38. Fujiwara K, Koyama K, Suga K, et al. A (90)Y-labelled anti-ROBO1 monoclonal antibody exhibits antitumour activity against hepatocellular carcinoma xenografts during ROBO1-targeted radioimmunotherapy. EJNMMI Res. 2014;4:29.
39. Liu Y, Yin Z, Xu X, et al. Crosstalk between the activated Slit2-Robo1 pathway and TGF-beta1 signalling promotes cardiac fibrosis. ESC Heart Fail. 2021;8:447-460.
40. Nikole R Zuñiga, Alexandre Dumoulin, Giuseppe Vaccaro, et al. Cables1 links Slit/Robo and Wnt/Frizzled signaling in commissural axon guidance. Development. 2023;150:dev201671.
41. Jinseol Rhee , Tim Buchan, Lawrence Zukerberg, et al. Cables links Robo-bound Abl kinase to N-cadherin-bound beta-catenin to mediate Slit-induced modulation of adhesion and transcription. Nat Cell Biol. 2007;9:883-892.
42. Zhang QQ, Zhou DL, Lei Y, et al. Slit2/Robo1 signaling promotes intestinal tumorigenesis through Src-mediated activation of the Wnt/beta-catenin pathway. Oncotarget 2015;6:3123-35.
43. Poh AR, Ernst M. Functional roles of SRC signaling in pancreatic cancer: Recent insights provide novel therapeutic opportunities. Oncogene 2023;42:1786-1801.
44. Dexing Fang , David Hawke, Yanhua Zheng, et al. Phosphorylation of beta-catenin by AKT promotes beta-catenin transcriptional activity. J Biol Chem. 2007;282:11221-9.
45. Ge WS, Wang YJ, Wu JX, et al. beta-catenin is overexpressed in hepatic fibrosis and blockage of Wnt/beta-catenin signaling inhibits hepatic stellate cell activation. Mol Med Rep. 2014;9:2145-51.
46. Aleksandrova N, Gutsche I, Kandiah E, et al. Robo1 Forms a Compact Dimer-of-Dimers Assembly. Structure. 2018;26:320-328 e4.
47. Kato S, Hikita H, Tsukamoto O, et al. Activation of the Integrin alphaV-YAP-CTGF Axis in Liver Sinusoidal Endothelial Cells Promotes Liver Fibrogenesis, Leading to Portal Hypertension and Liver Carcinogenesis in Congestive Hepatopathy. Gastroenterology. 2026;170:1000-1016.
48. Abreu JG, Ketpura NI, Reversade B, et al. Connective-tissue growth factor (CTGF) modulates cell signalling by BMP and TGF-beta. Nat Cell Biol. 2002;4:599-604.
49. Leask A, Hutchenreuther J. Activation of latent TGFbeta by alphavbeta 1 integrin: of potential importance in myofibroblast activation in fibrosis. J Cell Commun Signal. 2014;8:171-2.
50. Marcos-Mondejar P, Peregrin S, Li JY, et al. The lhx2 transcription factor controls thalamocortical axonal guidance by specific regulation of robo1 and robo2 receptors. J Neurosci. 2012;32:4372-85.
51. Tao J, Wu Z, Liang Y, et al. Lhx2 specifically expressed in HSCs promotes liver regeneration and inhibits liver fibrosis. Hepatology. 2025;82:683-701.
52. Hendesi H, Barbe MF, Safadi FF, et al. Integrin mediated adhesion of osteoblasts to connective tissue growth factor (CTGF/CCN2) induces cytoskeleton reorganization and cell differentiation. PLoS One. 2015;10:e0115325.
53. Gao B, Arab JP, Liangpunsakul S, et al. Metabolic dysfunction and alcohol-associated liver disease (MetALD). eGastroenterology. 2025;3:e100319.
54. Gao H, Jiang Y, Zeng G, et al. Cell-to-cell and organ-to-organ crosstalk in the pathogenesis of alcohol-associated liver disease. eGastroenterology. 2024;2.
55. Chen L, Charrier AL, Leask A, et al. Ethanol-stimulated differentiated functions of human or mouse hepatic stellate cells are mediated by connective tissue growth factor. J Hepatol. 2011;55:399-406.